

# In-situ X-ray diffraction study on $\text{M}\text{Ini}_{3.75}\text{Co}_{0.75}\text{Mn}_{0.3}\text{Al}_{0.2}$ during electrochemical hydriding-dehydriding process<sup>①</sup>

YUAN Zhi-qing(袁志庆), LI Guang-lie(吕光烈), GU Jian-ming(顾建明),

TU Xiao-yan(屠小燕), WANG Xin-xi(王新喜)

(Central Laboratory, Zhejiang University, Hangzhou 310028, China)

**Abstract:** Phase transformations and lattice expansions of  $\text{M}\text{Ini}_{3.75}\text{Co}_{0.75}\text{Mn}_{0.3}\text{Al}_{0.2}$  during the electrochemical hydriding-dehydriding process were investigated using *in-situ* X-ray diffraction. An intermediate hydride  $\gamma$  phase between the hydrogen solid solution  $\alpha$  phase and fully hydrided  $\beta$  phase can be observed during the cycling. The formation of  $\gamma$  phase is related to the diffusion of hydrogen in the crystal grains. The lower the charge rate is, the higher the content of  $\gamma$  phase is. The phase transformations during the hydriding-dehydriding process can be described as  $\alpha = \alpha + \gamma + \beta = \beta = \gamma + \alpha = \alpha$ . The lattice expansion from  $\alpha$  to  $\beta$  is discrete, while that from  $\gamma$  to  $\beta$  is continuous. The formation of  $\gamma$  phase can reduce the discrete lattice expansion from  $\alpha$  to  $\beta$  by 30%.

**Key words:** *in-situ* X-ray diffraction; phase transformation; lattice expansion; intermetallic alloys; hydrides

**CLC number:** TG 139

**Document code:** A

## 1 INTRODUCTION

$\text{AB}_5$ -type intermetallic hydrides based on  $\text{LaNi}_5$  have been found in wide application as the negative electrodes in  $\text{NiMH}$  batteries. A representative and commercial one is  $\text{Mm}$  ( $\text{NiCoMnAl}$ )<sub>5</sub> ( $\text{Mm}$ : mischmetal, it's used only for financial reason). For many years, it has been investigated with great interest in details. Now,  $\text{AB}_5$ -type alloys and other type metal hydrides have been the most promising active electrode materials that can be efficiently used for electric vehicles.

However, the degradation of alloys in long term hydriding-dehydriding cycling is still a serious problem in practical use. It has been reported that this degradation is mainly induced by the pulverization of the alloys<sup>[1]</sup>. The lattice expansion is generally considered as the important factor that leads to the pulverization<sup>[2]</sup>. Furthermore, Notten et al<sup>[3]</sup> and Nakamura et al<sup>[4]</sup> found that the discrete  $\alpha$  to  $\beta$  lattice expansion rather than the total lattice expansion is thought to be the dominant factor that accelerates the pulverization. Although their findings are suitable for elucidating the behavior of alloys in the gas-solid reaction, it may not be good enough to interpret the behavior of the alloys as electrode during the charge-discharge process for the reason that H atoms diffuse in the grains is always kinetically limited, which has been proved by Latroche et al<sup>[5]</sup> and Chartouni et al<sup>[6]</sup>. They found a second hydride phase during the charge-discharge process, which has a positive effect

on the discrete lattice expansion.

In this paper, we present the results obtained by *in-situ* X-ray diffraction. The phase transitions and lattice expansions of  $\text{M}\text{Ini}_{3.75}\text{Co}_{0.75}\text{Mn}_{0.3}\text{Al}_{0.2}$  during the electrochemical hydriding and dehydriding process are discussed.

## 2 EXPERIMENTAL

### 2.1 Alloy preparation

An alloy ingot of  $\text{M}\text{Ini}_{3.75}\text{Co}_{0.75}\text{Mn}_{0.3}\text{Al}_{0.2}$  was prepared by frequency induction melting the La-rich mischmetal and high purity metals of Ni, Co, Mn, Al in an Ar atmosphere and annealing at 1 473 K for 10 h. The ingot was further grounded into the particle size of 30  $\mu\text{m}$  for X-ray diffraction measurements.

### 2.2 Electrode preparation

450 mg of active material was combined homogeneously with 75 mg of carbon black and 30 mg of PTFE solution (30%, mass fraction). Then, this mixture was cold pressured onto a nickel foam. The product so obtained had a diameter of 20 mm and thickness of 0.5 mm.

### 2.3 Electrochemical measurements

The electrodes were immersed in 6 mol/L KOH electrolyte. The potential was monitored against a  $\text{Hg}/\text{HgO}$  reference electrode. Before the *in-situ* XRD measurements, the electrode was activated by cycling several times at C/10 for 12 h and D/10 with a cut-

① Foundation item: Projects (50071052; 50131040) supported by the National Natural Science Foundation of China

Received date: 2003-05-28; Accepted date: 2003-11-10

Correspondence: Li Guang-lie, Professor; Tel: +86-571-88273491-15; E-mail: gllu@zju.edu.cn

off at 0.5 V vs Hg/HgO. For in-situ X-ray diffraction, the electrode was charged at 30, 45, and 60 mA/g, respectively. The discharge current is the same as that mentioned above, but with a cut-off at 0.5 V vs Hg/HgO.

#### 2.4 In-situ X-ray diffraction

X-ray powder diffraction measurements were performed on a Rigaku D/Max-2550/PC diffractometer operating at 40 kV and 300 mA. The divergence slit and the scattering slit were set to  $1^\circ$  and the receiving slit 0.15 mm. In order to perform the time-resolved X-ray diffraction, a special electrochemical cell was designed, which is described in Fig. 1. This cell was half-sealed and the negative electrode was tightly pressured to keep plain by a polyester film which was transparent to X-ray. Function of the sample plate was making the surface of the cathode lie on the datum plane, as in the ordinary X-ray

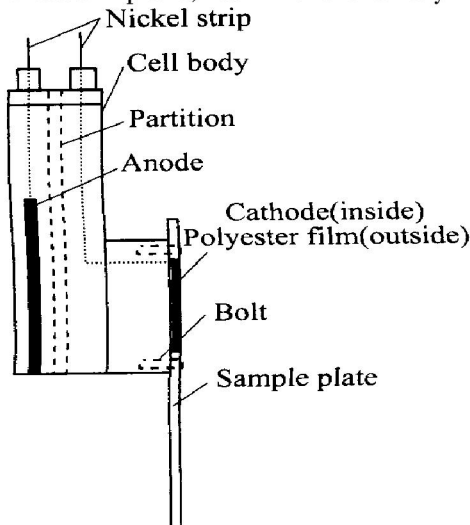


**Fig. 1** Description of electrochemical cell used in in-situ X-ray diffraction measurements

diffraction measurement. Intensity of (111) peak so obtained was not less than  $1.5 \times 10^4$  counts at the scan speed of  $0.4^\circ/\text{min}$ .

#### 2.5 XRD patterns analysis

The Rietveld refinement software we used is MAUD<sup>[7]</sup>, which is suitable for anisotropic profile broadening analysis. The precise lattice constants and phase abundance in the cycling were obtained by Rietveld refinement.

### 3 RESULTS

In-situ X-ray diffraction patterns during the hydriding-dehydriding process are shown in Fig. 2. From it we can see that when  $x_{\text{H}}(\text{H/M}) = 0.6$  and below, the mainly phases are the solution solid ( $\alpha$ ) and the remaining phase, though these two phases are difficult to be distinguished. As the hydriding process going on, two other phases begin to appear. The one with larger lattice constants is the commonly recognized hydride phase, namely  $\beta$  phase, while the other with smaller lattice constants is newly found by Lartroche et al<sup>[5]</sup> in the charging process, which is named as  $\gamma$  phase. Although the  $\gamma$  phase is a hydride phase, its content decreases as the hydriding process going on. This characteristic is very different from another hydride phase ( $\beta$ ), whose content keeps increasing through the hydriding process. At the end of hydriding, the  $\beta$  phase is dominant, but a little solid solution phase and remaining phase still exist.

In the dehydriding process, there are two incorporations occurred. One is the  $\beta$  phase immersed into  $\gamma$  phase and one is the solid solution phase incorporated into the remaining phase. When the dehydriding process is finished, the hydrides disappear and the

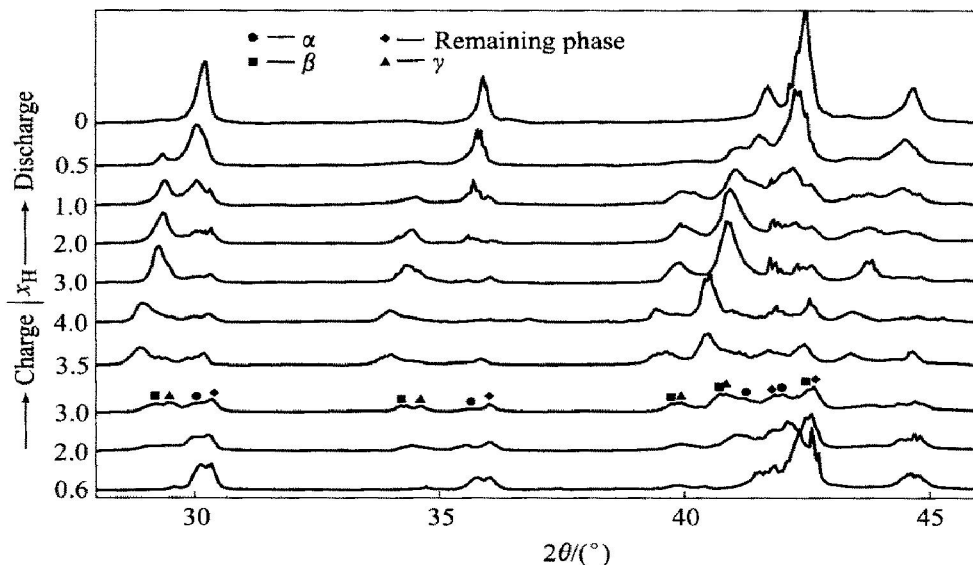


**Fig. 2** In-situ X-ray diffraction patterns in charge-discharge process  
(The value of  $x_{\text{H}}(\text{H/M})$  is approximate. The charge rate is 30 mA/g)

solid solution phase resumes being the state of that before hydriding, as seen in Fig. 2.

During the hydriding process, the cell volume expansions of  $\alpha$ ,  $\beta$  and  $\gamma$  phases can be clearly observed from Fig. 3. It can be found that the cell volume of  $\alpha$  phase is much smaller than those of  $\beta$  and  $\gamma$  phases. So, this type of cell volume expansion is discrete. However, the volume expansion between  $\gamma$  and  $\beta$  phases is somewhat continuous. Another lattice expansion details can also be found in Fig. 3. After  $\beta$  phase appears, the cell volume of  $\alpha$  and  $\gamma$  phases both decrease until the charge process completes. For  $\alpha$  phase, the change in volume in dehydriding process is reverse to that in the hydriding process.

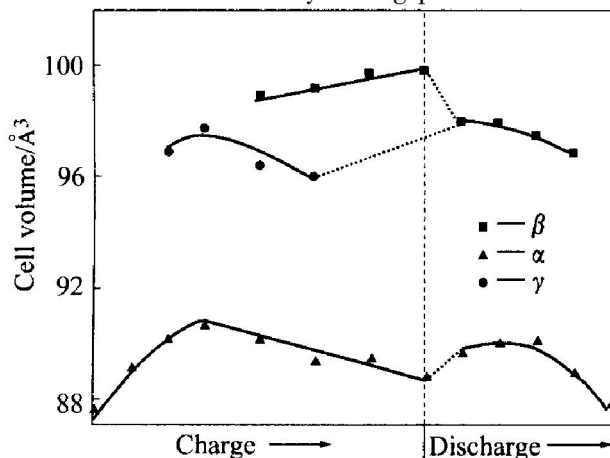


Fig. 3 Cell volume expansion in charge-discharge process

From Fig. 4, it can be concluded that the way of expanding of  $a$ -axis and  $c$ -axis of  $\beta$  phase is different. During the hydriding process, the  $c$ -axis is the first to expand and the  $a$ -axis is the second, while during the dehydriding process, the  $c$ -axis drops more quickly than  $a$ -axis does.

In order to investigate the effect of the diffusion of H atom on the hydriding-dehydriding process, the contents of the remaining phase and  $\gamma$  phase which

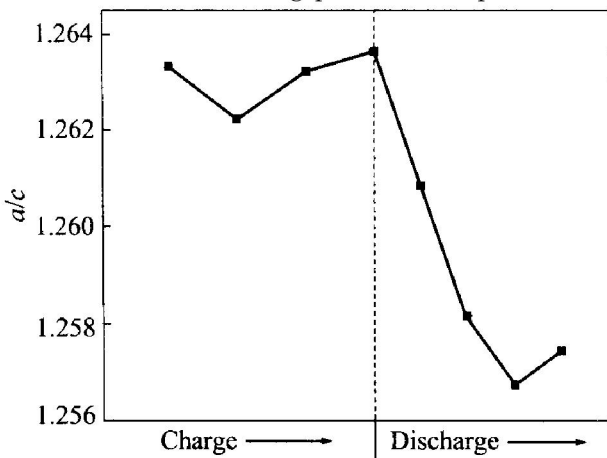


Fig. 4 Anisotropic lattice expansion of  $\beta$  phase in charge-discharge process

were obtained under different electrochemical conditions were compared. They are shown in Fig. 5. It is clearly indicated that at the lower charge rate, which is near to equilibrium, the content of remaining phase is much lower, while that of  $\gamma$  phase is higher. It seems that the diffusion of H atom in the grains has a great effect on the formation of those phases.

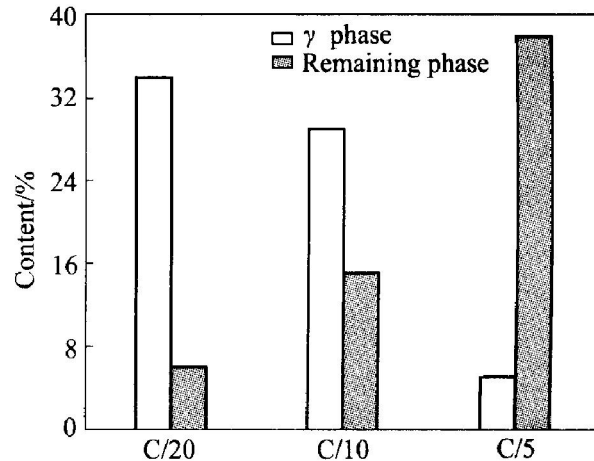


Fig. 5 Phase abundances for samples charged at different rate, but with same H content ( $x_H(H/M) = 0.3$ )

## 4 DISCUSSION

### 4.1 Phase transformation

During the hydriding-dehydriding process, the content of  $\gamma$  phase has a maximum value about  $x_H(H/M) = 3.0$ . So the composition of this phase is about  $Mn_{1.75}Ni_{0.75}Co_{0.75}Al_{0.2}H_{3.0}$ . The structure of this phase has a hexagonal symmetry, which is the same as that of solid solution phase and  $\beta$  phase. For the reason that the  $\gamma$  phase is an intermediate one between  $\alpha$  and  $\beta$  phases, it can be supposed that the  $\gamma$  phase also has the structure with space group of P6/mmm. Fig. 6 represents the observed, calculated lines and the difference plot between them. From it we can conclude that all of the phases having the same structure is reasonable.

Fig. 5 indicates that the  $\gamma$  phase can only be formed when the charge rate is very low, which is close to equilibrium. By considering this, the  $\gamma$  phase may be related to the diffusion of H atom in the grains and we can suppose that the distribution of H content in the grains is discontinuous. In the region that is close to the grain surface, there is a high over pressure and the H content at there is also high, then the  $\beta$  phase is formed; while in the region that is far from the surface, the content of H is low, so the  $\gamma$  phase with lower lattice constants is produced, as described in Fig. 7. Because there are several interstitial sites for H to occupy in the  $CaCu_5$  structure<sup>[8]</sup>, the  $\gamma$  phase may be formed when the certain preferred sites are occu-

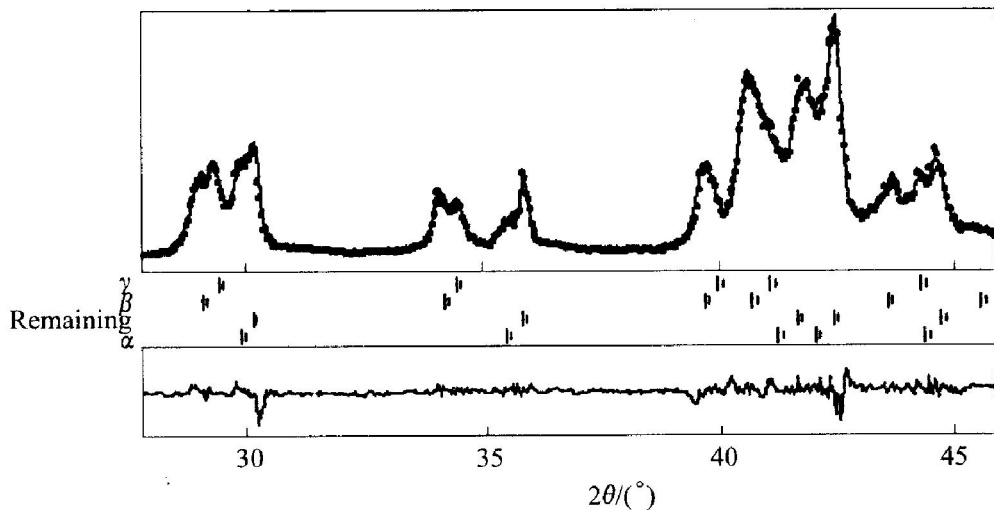


**Fig. 6** Parts of observed, calculated lines and difference plot obtained by Rietveld refinement for sample of  $x_{\text{H}}(\text{H}/\text{M}) = 3.0$   
( $2\theta$  range of whole pattern is from  $18^\circ$  to  $100^\circ$ )

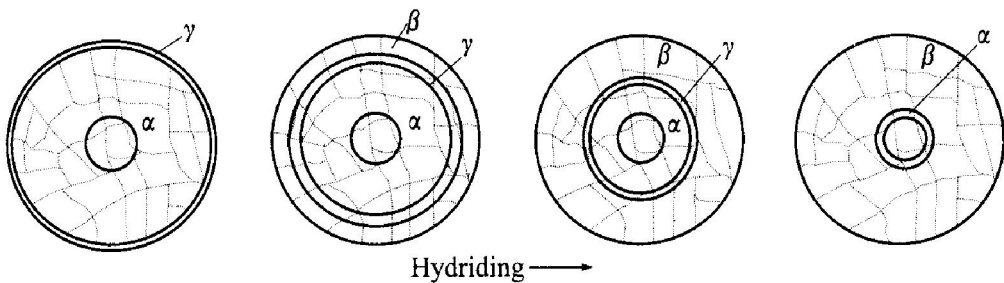


**Fig. 7** Schematic description of hydriding process within a grain  
(The almost unchanged core of the grain represents the remaining phase)

pied by H, while the  $\beta$  phase is produced when the most of the interstitial sites are occupied. According to Percheron-Guégan et al<sup>[9]</sup>, the  $\gamma$  phase is formed when the content of Co excesses 10% or the alloy has a nonstoichiometric composition. By considering this, it can be concluded that the alloys with the above characteristic can produce some certain interstitial sites that are suitable for the occupancy of H, which can induce the formation of  $\gamma$  phase. And the  $\gamma$  phase can be considered as a stable intermetallic phase.

As the charge process continues, most of the preferred interstitial sites are occupied by hydrogen. So the  $\gamma$  phase disappears and the content of the  $\beta$  phase continuously increases. Unlike  $\beta$  phase, the  $\alpha$  phase has a decreasing in content, but still keeps a little at the end of hydriding process. But for the remaining phase, the change in its abundance is weak. It may be induced by the diffusion of H, because H cannot reach the core of the grains, as shown in Fig. 7.

At the beginning of the dehydriding process, there is a drop of cell volume of the  $\beta$  phase. After that, the  $\beta$  and  $\gamma$  phases immerge into one. This can be understood that the content of H in the grain is reduced and H occupies the sites that can produce  $\gamma$

phase. The remaining phase can be incorporated into  $\alpha$  phase completely at the end of dehydriding process. So, the phase transitions in the charge-discharge process can be described as (the remaining phase excluded):  $\alpha \rightleftharpoons \gamma + \beta \rightleftharpoons \beta \rightleftharpoons \gamma + \alpha \rightleftharpoons \alpha$ .

#### 4.2 Lattice expansion

As can be seen in Fig. 3, there is a discrete lattice expansion between  $\alpha$  to  $\beta$  and  $\alpha$  to  $\gamma$ , but the lattice expansion of  $\gamma$  to  $\beta$  is somewhat continuous. However, because the coexistence of the  $\gamma$  phase, the discrete expansion between  $\alpha$  to  $\beta$  can be released by about 30%. From Fig. 3, it can also be found that when the  $\beta$  precipitates grow up, the volume of  $\alpha$  phase and  $\gamma$  phase begins to decrease. The reason accounts for this may be that in the hydriding process, high density dislocation is generated by the strain<sup>[10, 12]</sup>, which results in lots of vacancies. It is believed that the vacancy can induce the decreasing of lattice constants. This changes of lattice constants are reversible in the whole cycling process, as shown in Fig. 3.

The changes of  $a$ -axis and  $c$ -axis of  $\beta$  phase are anisotropic as shown in Fig. 3. This may be affected by the sites that hydrogen prefers to occupy<sup>[13]</sup>. According to Andresen et al<sup>[14]</sup>, the interstitial sites in-

cluded in the  $\text{LaNi}_5$ -type alloys can be classified into  $D_1$  site and  $D_2$  site. At the first stage,  $D_2$  site (near the  $Z = 1/2$  plane and corresponding to 6 m, 4 h, and 12o sites in the five-site model<sup>[15]</sup>) is easy to be occupied which will increase the  $c$ -axis, and after a part of  $D_2$  site is occupied, the  $D_1$  site (near the  $Z = 0$  plane and corresponding to 3f and 12n sites in the five-site model<sup>[15]</sup>) begins to be occupied by hydrogen, which will induce the increasing of the  $a$ -axis. This also can be reversed during the dehydriding process that  $a$ -axis is the first to decrease and then the  $c$ -axis.

## 5 CONCLUSION

The diffusion of hydrogen in the grains has a great effect on the phase transformations of  $\text{M1Ni}_{3.75}\text{Co}_{0.75}\text{Mn}_{0.3}\text{Al}_{0.2}$  in the charge-discharge process. When the charge rate is low, the coexistence of two hydride phases, namely, the partially hydrided phase ( $\gamma$ ) and the fully hydrided phase ( $\beta$ ), occurs. The phase transformations can be described as  $\alpha \rightleftharpoons \gamma + \beta \rightleftharpoons \beta \rightleftharpoons \gamma + \alpha \rightleftharpoons \alpha$ . Because of the existence of the  $\gamma$  phase, the discrete lattice expansion of  $\alpha$  to  $\beta$  can be released by about 30%. Another effect of the diffusion of hydrogen on the phase transformations is that the solid solution phases cannot be completely removed by the hydriding process. Consequently, higher capacity and smaller discrete lattice expansions can be obtained at low charging rate.

## REFERENCES

- [1] Willems J J G. Metal hydride electrodes stability of  $\text{LaNi}_5$ -related compounds [J]. Philips J Res, 1984, 39: 1–94.
- [2] Sakai T, Oguro K, Miyamura H, et al. Some factors affecting the cycle lives of  $\text{LaNi}_5$ -based alloy electrodes of hydrogen batteries [J]. J Less-Common Met, 1990, 161: 193–202.
- [3] Notten P H L, Daams J L C, Einerhand R E F. On the nature of the electrochemical cycling stability of nonsto-

chiometric  $\text{LaNi}_5$ -based hydride-forming compounds: (part II) *in situ* X-ray diffraction diffractometry [J]. J Alloys Comp, 1994, 210: 233–241.

- [4] Nakamura Y, Sato K, Fujitani S, et al. Lattice expanding behavior and degradation of  $\text{LaNi}_5$ -based alloys [J]. J Alloys Comp, 1998, 267: 205–210.
- [5] Latroche M, Percheron Guégan A, Chabre Y. Influence of cobalt content in  $\text{MmNi}_{4.03-x}\text{Mn}_{0.3}\text{Al}_{0.4}\text{Co}_x$  alloy ( $x = 0.36$  and  $x = 0.69$ ) on its electrochemical behaviour studied by *in situ* neutron diffraction [J]. J Alloys Comp, 1999, 293–295: 637–642.
- [6] Chartouni D, Gross K. Phase transitions in  $\text{LaNi}_4\text{Co}$  during electrochemical cycling: an *in situ* X-ray diffraction study [J]. J Electrochem Soc, 2001, 148 (3): A241–A248.
- [7] Lutterotti L, Scardi P. Simultaneous structure and size strain refinement by the Rietveld method [J]. J Appl Cryst, 1990, 23: 246–252.
- [8] Westlake D G. Hydrides of intermetallic compounds: A review of stabilities, stoichiometries and preferred hydrogen sites [J]. J Less-Common Met, 1983, 91: 1–20.
- [9] Latroche M, Chabre Y, Percheron Guégan A. Influence of stoichiometry and composition on the structural and electrochemical properties of  $\text{AB}_{5+y}$ -based alloys used as negative electrode materials in  $\text{Ni}-\text{MH}$  batteries [J]. J Alloys Comp, 2002, 330–332: 787–791.
- [10] Cerny R, Joubert J M, Lartroche M, et al. Anisotropic diffraction peak broadening and dislocation substructure in hydrogen-cycled  $\text{LaNi}_5$  and substitutional derivatives [J]. J Appl Cryst, 2000, 33: 997–1005.
- [11] Kim G, Lee S, Lee K, et al. Observation of the defects induced by hydrogen absorption and desorption in  $\text{LaNi}_5$  [J]. Acta Metall Mater, 1994, 42(9): 3157–3161.
- [12] Kim G, Lee S, Lee K, et al. TEM study on the nucleation and growth of hydride in  $\text{LaNi}_5$  alloy [J]. Acta Metall Mater, 1995, 43(6): 2233–2240.
- [13] Ono E, Nomura K, Akiba E, et al. Phase transformations of the  $\text{LaNi}_5\text{H}_2$  system [J]. J Less-Common Met, 1985, 113: 113–117.
- [14] Andresen A F. Structure and phase relations in metal hydrides studied by neutron diffraction [J]. J Less-Common Met, 1982, 88: 1–8.
- [15] Percheron Guégan A, Lartigue C, Achard J C. Correlations between the structural properties, the ability and the hydrogen content of substituted  $\text{LaNi}_5$  compounds [J]. J Less-Common Met, 1985, 109: 287–309.

(Edited by YUAN Sai-qian)